Advances in Nano Research, *Vol. 19, No. 1 (2025) 1-11*
https://doi.org/10.12989/anr.2025.19.1.001

Comparative evaluation of commercial and natural nanoparticle adsorbents for efficient arsenic removal: Insights from kinetic modeling

Yelda Meyva-Zeybek*[1,2,3], Süer Kürklü-Kocaoğlu[1,4], Nilay Gizli[1] and Mustafa Demircioğlu[1]

[1]*Department of Chemical Engineering, Ege University, Izmir, Türkiye*
[2]*Department of Metallurgical and Materials Engineering, Mugla Sitki Kocman University, Mugla, Türkiye*
[3]*Department of Metallurgical and Materials Engineering, Karamanoglu Mehmetbey University, Karaman, Türkiye*
[4]*Department of Chemical Engineering, University of Texas at Austin, Austin, TX, U.S.A.*

(*Received October 29, 2024, Revised May 10, 2025, Accepted June 19, 2025*)

Abstract. Arsenic, which is a toxic substance in the human body, has attracted great interest due to high levels in drinking water supplied from underground resources. Novel separation methods for arsenic removal perform innovative products developed using nanomaterials. In this study, batch experiments were conducted for Adsorbsia GTO to obtain kinetics and mechanisms of As(V) sorption, and then they were compared to commercially available adsorbent MTM® and natural minerals named hematite (Fe_2O_3), goethite (FeOOH), and manganese dioxide (MnO_2). Adsorbsia GTO fitted slightly better to the Freundlich Isotherm with high adsorption capacity of 27.25 mg/g at pH 4. MnO_2 fitted to the Langmuir Isotherm very well and resulted in the highest adsorption capacity of 0.72 mg/g in natural oxides. The kinetics of all materials were modeled with "Infinite Solution Volume" and "Unreacted Core" models to understand reaction kinetics. Adsorbsia GTO fitted to models of "liquid film diffusion" and "chemical reaction" with over 0.98 of R^2 value. Column studies showed that Adsorbsia GTO had breakthrough and total exchange capacities of 26.5 and 84.4 mg/ml, respectively. As a natural alternative, MnO_2 with breakthrough and total exchange capacities of 4.3 and 14.2 mg/ml, fitted the models of "particle diffusion" and "reacted layer" in natural minerals.

Keywords: adsorbsia GTO, adsorption kinetics, arsenic removal, manganese dioxide, natural mineral oxides, water treatment

1. Introduction

Arsenic is present in different compounds with various oxidation numbers, such as arsenate (As^{5+}), arsenite (As^{3+}), arsenic (As^0) and arsine (As^{3-}). It is usually present in As^{5+} form in water, but it is likely to be present as As^{3+} in anaerobic conditions (Smedley and Kinniburgh, 2002). In surface waters, the dominant arsenic species are $H_2AsO_4^-$, $HAsO_4^{2-}$, and AsO_4^{3-} with arsenic having 5+ valence. In aqueous solutions, the equilibrium constants (pK_a) for As(V) are given as follows (Chen *et al.* 2019) and the speciation of arsenic in aqueous solutions with respect to pH is controlled by these equilibrium constants. Fig. 1 shows that the change in speciation of arsenic at various pH values. As pH increases from 0 to 14, the species of arsenic changes drastically. While H_3AsO_4 is the dominant species below pH value of 2.2, it dissociates into $H_2AsO_4^-$ and H_3O^+ beyond this pH value. Similarly, $H_2AsO_4^-$ and $HAsO_4^{2-}$ dissociates into different arsenic species at pH values higher than their pK_a values.

$$H_3AsO_4 + H_2O \leftrightarrow {H_2AsO_4}^- + {H_3O}^+ \quad pK_{a1} = 2.20 \quad (1)$$

$${H_2AsO_4}^- + H_2O \leftrightarrow {HAsO_4}^{2-} + {H_3O}^+ \quad pK_{a2} = 6.97 \quad (2)$$

$${HAsO_4}^{2-} + H_2O \leftrightarrow {AsO_4}^{3-} + {H_3O}^+ \quad pK_{a3} = 11.53 \quad (3)$$

Arsenic is mostly present at concentrations of less than 1–2 µg/l in natural waters whereas the arsenic concentration in groundwaters can increase significantly up to 12 mg/l due to sulfide mineral deriving from volcanic rocks. So, food and drinking water are the most significant routes of arsenic exposure, including beverages that are made from drinking water (WHO 2022). The consumption of arsenic in drinking water has undesired effects on human health in short- or long-term exposure. In the short term, stomachache, vomiting and diarrhea can occur after drinking arsenic-contaminated water, and high arsenic poisoning may even cause numbness, cramping in muscles, and death (Altowayti *et al.* 2022). For long-term exposure, dermal lesions, peripheral vascular disease, and lung cancer have been encountered in populations ingesting arsenic polluted water (WHO, 2022). Moreover, respiratory infections, delays, or birth defects are found in pregnant women who were exposed to arsenic (Abdul *et al.* 2015, van Halem *et al.* 2009) and the activation of many human body enzymes is restricted by arsenic causing liver and renal damage (Mandal and Suzuki 2002). Due to these side effects of arsenic on human health, the permissible level of arsenic has been reduced from 50 to 10 µg/l by the World Health Organization (WHO) (Alka *et al.* 2021, Choong *et al.* 2007). Arsenic pollution has been detected in some Asian countries, including Taiwan, Pakistan, Myanmar, India, and Bangladesh whereas arsenic contamination in drinking water was also reported in a few South American countries

*Corresponding author, Assistant Professor,
E-mail: yeldameyva@gmail.com

ISSN: 2287-237X (Print), 2287-2388 (Online)

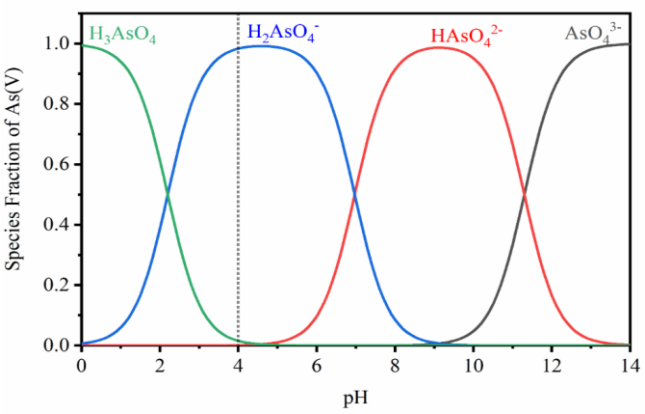

Fig. 1 Concentrations of As(V) species H_3AsO_4, $H_2AsO_4^-$, $HAsO_4^{2-}$, and AsO_4^{3-} at different pH values (Plotted from pKa values from Chen *et al*. 2019)

such as Mexico, Colombia, Chile, and Peru (Altowayti *et al*. 2022).

The wastewater treatment methods are classified into three groups as precipitation, adsorption and membrane technology which includes reverse osmosis, nanofiltration, and electrodialysis. Most of these arsenic removal techniques need a lot of energy and reagents, so they can be costly (Altowayti *et al*. 2022). Precipitation is a simple and cost-efficient process, however, it needs arsenite peroxidation and produces highly toxic sludge (Ungureanu *et al*. 2015). Membrane technology is so effective for arsenic removing, but it has very high capital, maintenance, and operational costs (Mohan and Pittman 2007). Therefore, adsorption is one of the most prominent techniques for elimination of arsenic from water. The arsenic species can interact with suitable adsorbents physically or chemically. Physical adsorption is caused by the Van der Waals forces which can be certainly broken by calcination or sonication. Different types of adsorbents for arsenic adsorption were reported in literature. Especially, nanoparticles have a significant role as adsorbents in the wastewater treatment such as nano-particles of magnetic SiO_2-coated (Mehryar and Marandi 2024), iron which is synthesized with Genovese basil extract (Fu *et al*. 2023), TiO_2 (Aitbelale *et al*. 2023), calcium oxide (Eddy *et al*. 2023) due to their high surface-to-area ratio. Iron-based nanoparticles are effective in arsenic adsorption (Carneiro *et al*. 2022, Diephuis *et al*. 2022, Hristovski *et al*. 2008, Jeon *et al*. 2009, Kundu and Gupta 2007, Mayo *et al*. 2007, Streat *et al*. 2008, Zhang *et al*. 2003). Carneiro *et al*. (2022) found that maximum adsorption capacities of iron-coated cork granulate for arsenic removal were 4.2 mg/g at pH 3 and 1.6 mg/g at pH 9, respectively. The clusters of iron oxide nanoparticles (cIONPs) have higher adsorption capacity than other IONPs with 121.4 mg/g (Diephuis *et al*. 2022). Iron-coated zeolite and cement were also suggested as suitable materials for the treatment of wastewater containing As(V) and As(III) with adsorption capacities of 0.68 and 0.69 mg/g, respectively (Jeon *et al*. 2009, Kundu and Gupta 2007). Arsenic adsorption was also affected by nanoparticle size. For instance, the arsenic adsorption capacity of magnetite increased almost 200 times by reducing particle size from 300 to 12 nm (Mayo *et al*. 2007). The pH level of arsenic contaminated water also affects the sorption capacity of iron-based nanoparticles (Carneiro *et al*. 2022, Kundu and Gupta 2007, Streat *et al*. 2008, Zhang *et al*. 2003).

Adsorption properties of iron oxide were enhanced by hybridizing with inorganic/organic polymers for removal of arsenic (DeMarco *et al*. 2003, Iesan *et al*. 2008, Möller and Sylvester, 2008). Katsoyiannis and Zouboulis (2002) used modified polymeric materials such as polystyrene and polyHIPE, which is a novel microporous material by polymerization of a high internal phase emulsion. They coated the surface of polymeric material by using suitable adsorbing agents to remove the arsenic anions. PolyHIPE was found to be an effective adsorbent. However, there are many challenges with synthesis and application of ideal polymeric adsorbents for environmental concerns and molecular design (Pan *et al*. 2009).

Dutta *et al*. (2004), Haron *et al*. (2006), and Nabi *et al*. (2009) investigated the arsenic sorption capacity of titanium dioxide (TiO_2) nanoparticles at various pH levels. Pena *et al*. (2005) studied the effectiveness of nanocrystalline TiO_2 in sorption of As in the presence of foreign anions whereas Xu and Meng (2009) investigated the size effects of nanocrystalline TiO_2. The adsorption capacity of TiO_2 for arsenic species linearly increased by increasing the BET surface area of particles. Furthermore, Hristovski *et al*. (2008) studied various metal oxides including TiO_2 and compared them with commercial adsorbents, Adsorbsia GTO and MetsorbG. They found out Adsorbsia GTO, with a high adsorption capacity of 28.5 mg/g at pH level of 8.4, fitted the Freundlich Isotherm well. While there are various studies in literature that examine the adsorption isotherms of Adsorbsia GTO, the kinetic behavior of adsorbents and column studies are key factors in determining its overall performance. A comprehensive understanding of the adsorption kinetics, mechanisms as well as the performance of Adsorbsia GTO in column mode operation is essential to optimize its arsenic removal efficiency and enable its effective implementation in water treatment applications. Moreover, hematite, magnetite, and goethite containing iron oxides are natural sources for arsenic removal. According to sorption kinetics, the equilibrium was reached in less than 2 days for all adsorbents, and it was more rapid for goethite and magnetite than for hematite. The adsorption capacity of arsenic decreased onto these natural adsorbents at alkaline pH values. Hematite had the highest sorption capacity for As(III) compared to goethite and magnetite (Giménez *et al*. 2007). Mamindy-Pajany *et al*. (2011) claimed that zero-valent iron had the highest adsorption rate and magnetite, hematite, and goethite followed it, respectively.

In literature, there is also a limitation of kinetic studies focusing on the mass transfer mechanism underlying adsorption of arsenic although several studies are available concentrated on applying simplified kinetic models like “pseudo-first-order” and “pseudo-second-order”, to identify the adsorption kinetics (McGeogh *et al*. 2024). However, it is known that the adsorption mechanism is more complicated, involving multiple diffusional steps.

To the best of our knowledge, studies have mostly focused on iron-based nanoparticles in literature. There are very limited studies on arsenic adsorption kinetics, mechanism

Table 1 Chemical and Physical Properties of Adsorbsia GTO (Dow Chemical Company)

Property		Unit	Value
Particle Size	On 10 mesh	%	<5
	Through 60 mesh	%	<10
Moisture Content		%	<15
As(V) Equilibrium Capacity* (@50 ppb, pH 7, room temperature)		g/kg	12-15

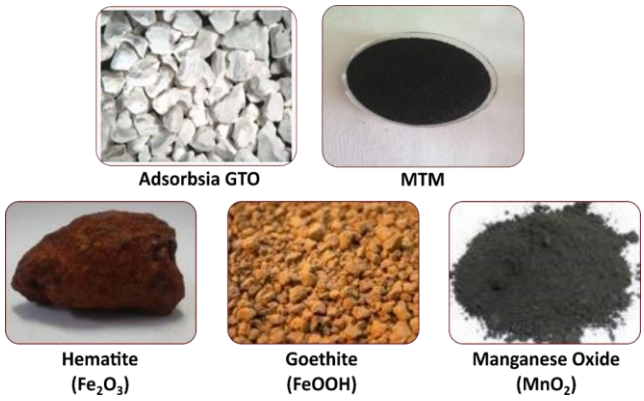

Fig. 2 Physical structures of commercially available and natural adsorbents

and column studies of Adsorbsia GTO, MTM® and natural metal oxides. In this study, arsenic was chosen as a target contaminant due to its inherent health and regulatory concerns. The adsorption capacities of commercially available aggregated nanosized materials, Adsorbsia GTO and MTM® were evaluated and compared with natural metal oxides, hematite (Fe_2O_3), goethite (FeOOH), and manganese dioxide (MnO_2). The arsenic adsorption studies conducted by a series of batch and fixed bed column studies. Moreover, the kinetic and equilibrium behavior of the adsorbents is crucial for the optimizing of the adsorption process design and operation. For this purpose, five different kinetic models were fitted to understand the mass transfer mechanisms and to identify the rate determining step which are film diffusion, particle diffusion or chemical reaction.

2. Materials and methods

Adsorbsia GTO (Dow Chemical) and MTM® (Clark Corp.) are commercially available adsorbents. The detailed properties of Adsorbsia GTO are given in Table 1. To investigate the morphological structure and determine the specific surface area of Adsorbsia GTO, scanning electron microscopy (SEM) (Zeiss GeminiSEM 500) and Brunauer-Emmett-Teller (BET) analyses were also conducted, respectively. SEM analysis was performed at magnifications of 5000x and 50000x with 5 kV. ImageJ was used to determine the average diameter of Adsorbsia GTO and the diameter of 200 particles are counted in the SEM image.

MTM® is purple black (dark brown) filter media based on granular manganese dioxide and capable of handling arsenic, iron, manganese, hydrogen sulfide and radium by oxidation and filtration. Iron- and manganese-based natural minerals hematite (Fe_2O_3), goethite (FeOOH), and manganese dioxide (MnO_2) were kindly supplied by the Department of Geophysical Engineering at Dokuz Eylül University, Türkiye. The physical structures of commercially available and natural adsorbents were given in Fig. 2.

As usual practice in the treatment of Adsorbsia GTO, particles were sieved and washed with 2L of distilled water and dried at 105°C in the oven. All natural mineral oxides were crushed and sieved. The particle size range between 0.50 and 0.71 mm was used.

All pH adjustments have been performed with 1M HCl (12M, Merck, Germany) solution and the pH meter (Thermo, Orion 4 Star) is used to measure the pH of solution. The As(V) solutions were prepared from sodium arsenate heptahydrate ($Na_2HAsO_4 \cdot 7H_2O$, Analytical grade, Merck). The concentration of As(V) ion in aqueous solution has been determined via Atomic Absorption Spectrophotometer (AAS, Varian 10 Plus) with the lower detection limit of 3 ppm. The working conditions of AAS were the wavelength of 193.7 nm with 10 mA lamp current and the slid width of 0.5 mm. Its fuel and support gas were acetylene and nitrous oxide, respectively. Sample solutions were prepared by using the blue band filter paper to remove particles from the solution for AAS analysis. Both batch and fixed bed column studies were shown schematically in Fig. 3. The maximum amount of adsorbent, pH effect and equilibrium and kinetics studies were done as batch operation (Fig. 3a) while column studies were done as continuous operation (Fig. 3b).

2.1 Batch studies

2.1.1 Determination of the maximum amount of adsorbent

Different amounts of adsorbent, 0.05, 0.1, 0.2, 0.4, 0.5 and 0.8 g were contacted with 50 ml of As(V) solution having concentration of 100 ppm for 24 hours at 25°C, adjusting the pH to 4, ensuring that only H_2AsO_4 species were present in the solution.

2.1.2 Effects of pH on arsenic adsorption

The adsorbent of 0.1 g has been contacted with 50 ml of As(V) solution having concentration of 100 ppm at five different pH values of 4, 6, 7, 8 and 10 for 24 hours at 25°C.

2.1.3 Equilibrium studies

The adsorbent of 0.1 g has been contacted with 50 ml of solutions having different As(V) concentrations such as 10, 25, 50, 75, 100 and 150 ppm for 24 hours at pH value of 4 and 25°C.

2.1.4 Kinetic studies

Sorption rates and mechanisms were determined by using adsorbent concentration of 2 g/l with 350 ml of 100 ppm As(V) solution and many samples were collected within 24 hours.

2.2 Continuous studies

These studies were carried out on 15 mm diameter

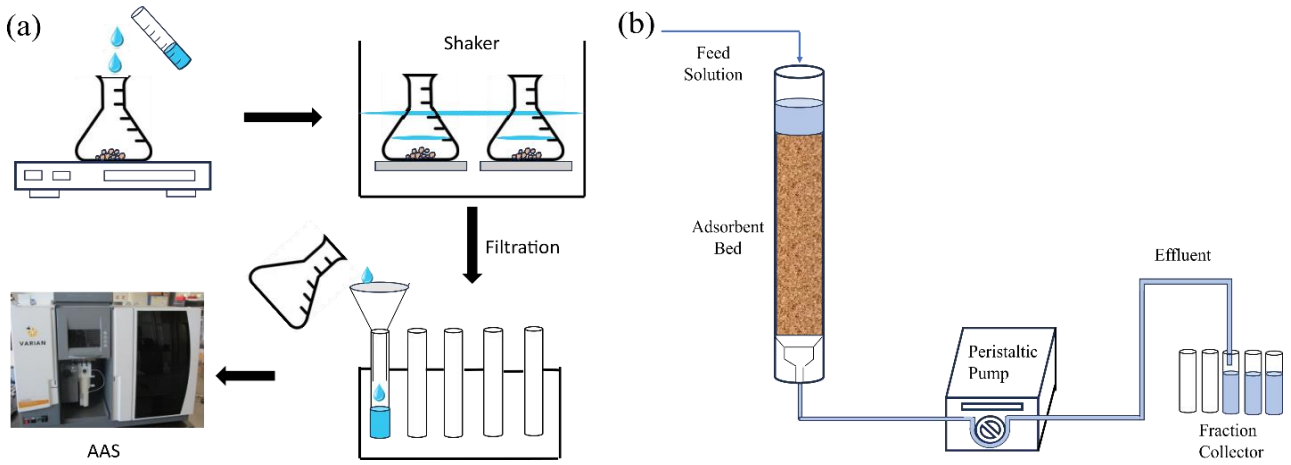

Fig. 3 Schematic representation of the (a) batch studies and (b) fixed bed column studies

columns with a bed volume of 14 ml. As(V) concentrations of 100, 200 and 300 ppm were used to compare different feed solutions in the column. Breakthrough curves were obtained for the best performing commercial and natural absorbents Adsorbsia GTO and MnO_2, respectively.

2.3 Equilibrium models

There are several types of equilibrium and kinetic models available to determine the thermodynamic and kinetic behavior of adsorbents for As(V) sorption from the water. The Langmuir and Freundlich adsorption models are developed mathematical models to quantify adsorption process. The Langmuir model is the theoretical model for monolayer adsorption. Both physical and chemical adsorption have been described by the Langmuir model, which was first created to characterize and quantify chemisorption on a collection of unique localized adsorption sites.

The solid phase adsorbate concentration (q_e) and the equilibrium liquid adsorbate concentration (C_e) are related by the Langmuir equation as follows:

$$q_e = \frac{QbC_e}{1 + bC_e} \tag{4}$$

where Q refers to the "maximum adsorption capacity" for the solid phase loading and b is "energy constant" related to adsorption heat (Ruthven, 1984). The linearized Langmuir equation is shown to determine the Langmuir constants from the experimental data as follows:

$$\frac{1}{q_e} = \frac{1}{Q} + \frac{1}{bQ}\frac{1}{C_e} \tag{5}$$

The Freundlich model is also a mathematical model used to quantify adsorption reactions and identify the adsorption equilibria. Adsorption is described by the Freundlich model in terms of the concentration of the adsorbate (Dutta *et al*. 2004).

$$q_e = kC_e^{\frac{1}{n}} \tag{6}$$

$$lnq_e = lnk + \frac{1}{n}lnC_e \tag{7}$$

where k and n are Freundlich constants and these values are derived from experimental data by plotting the linearized form of Equation (6) by plotting ln q_e, against ln C_e the intercept gives ln *k* and the slope is equal to *1*/*n*.

2.4 Adsorption Kinetics

Although there are several types of adsorption kinetic models, this study includes two of them called the "Infinite Solution Volume Diffusion Model" and "Unreacted Shrinking Core Model" (Kabay *et al*. 2003). Both of these models explain diffusion in fluid film and in the particle while the latter one (UCM) also considers chemical reaction as a rate limiting step. The concentration profiles change according to different mechanisms, and they are shown in Fig. 4. The concentration change is in the fluid film if the rate limiting step is film diffusion, while it is inside the particle (adsorbent) if the controlling step is particle diffusion. When there is no concentration difference inside the particle or fluid film it means the rate limiting step is the chemical reaction.

2.4.1 Infinite Solution Volume Diffusion Model (ISV)

The rate is controlled by the slower of the two steps named particle diffusion (interdiffusion of counter ions within the adsorbents) and film diffusion (interdiffusion of counter ions in the film).

In the case of particle diffusion, the concentration difference in the film is negligible and film diffusion is faster than particle diffusion. Only the adsorbent beads contain the concentration gradient. The fixed charge concentration and the bead interdiffusion coefficient are roughly correlated with the exchange flux. Conversely, the flow is independent of the film's diffusion coefficient, solution concentration, and thickness, instead, it is inversely proportional to the bead radius. Low liquid phase concentration, good ion exchange capacity, low degree of crosslinking, and poor liquid agitation are favorable conditions for control by liquid-phase mass transfer.

By using the diffusion equations on the adsorption systems, rate laws can be obtained. Due to problems deriving from diffusion-induced electrical forces, selectivity, particular interactions, and swelling changes, the differential equations

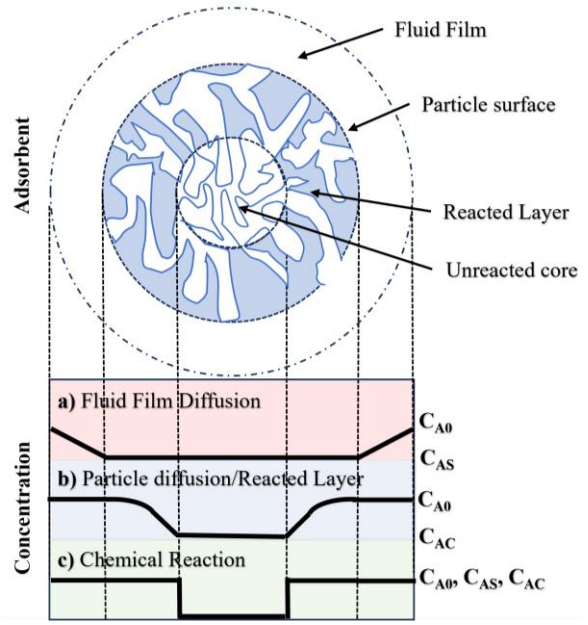

Fig. 4 Schematic representation of the concentration profiles during adsorption (a) Fluid film diffusion (b) Particle diffusion or Reacted Layer (c) Chemical reaction. C_{A0}: concentration in the bulk solution C_{AS}: concentration on the surface of particle C_{AC}: concentration on the surface of unreacted core

Table 2 Kinetic model equations for the adsorption

Method	Rate determining Step	Function (y-axes)	Transport characteristics
ISV	Particle diffusion	$-ln\,(1-X^2)$	$D_r = m\frac{r_0^2}{\pi^2}$
	Liquid film	$ln\,(1-X)$	$D = \frac{mr_0\delta\underline{C}}{(3C)}$
UCM	Fluid film	X	$K_{MA} = \frac{mar_0C_{s0}}{(3C_{A0})}$
	Reacted layer	$3-3(1-X)^{\frac{2}{3}}-2X$	$D_{e,r} = \frac{mar_0^2C_{s0}}{(6C_{A0})}$
	Chemical reaction	$1-(1-X)^{\frac{1}{3}}$	$k_s = \frac{mr_0}{C_{A0}}$

* m = slope of the function vs timeline

and boundary conditions are generally nonlinear. To overcome these complicated effects of nonlinear coupling of flux, the following diffusion kinetic treatments have been considered for idealized adsorption. Fick's first law usually describes the diffusion processes:

$$J_i = -D\nabla C_i \tag{8}$$

where J represents a diffusion flux, D and C are the diffusion coefficient and concentration, respectively.

Particle Diffusion

Within the adsorbent bead, concentration gradients will be present in the case of particle diffusion control. The rate laws are believed to be derived from a quasi-homogenous model. Diffusion in the solid phase is treated theoretically as passing through a homogenous spherical electrolyte gel.

$$-\,ln\,(1-X^2)\; = 2kt\; where\; k = \frac{D_r\pi^2}{r_0^2} \tag{9}$$

X is the "fractional attainment of equilibrium" defined as $\frac{(C_0-C_t)}{(C_0-C_e)}$, C_0 refers the initial concentration of As while C_t is the As concentration at time (t). r_o represents the bead radius and D_r is the diffusion coefficient.

Film Diffusion

Two assumptions can be made while deriving the rate laws for the film diffusion-controlled adsorption process: the film is assumed to be a planar layer and its interdiffusion to be quasi-stationary. If the film thickness is significantly less than the bead radius, this is acceptable.

$$ln\,(1-X)\; = kt\; where\; k = \frac{3DC}{r_0\delta\underline{C}} \tag{10}$$

D is the diffusion coefficient, r_0 is the radius at time zero, δ is the film thickness, C is the total concentration of both species A and B in solution and $\underline{C}$ is the total concentration of both species A and B in the resin phase.

2.4.2 Unreacted shrinking core model (shell progressive model)

The "Shell Progressive" or "Unreacted Shrinking Core" theories can explain the reaction when the adsorbent has a tiny porosity and is therefore essentially impermeable to the fluid reactant. In the shell progressive approach, it can be visualized that the following three steps occur in succession during reaction:

a. Mass transfer across the interface of the reactive species from the bulk solution to the solid bead's outer surface (Fluid Film Diffusion)

$$X = \frac{3C_{A0}K_{MA}}{ar_0C_{As}}t \tag{11}$$

b. The reaction zone is reached by the reacting species' interparticle diffusion from the outer surface through the reacted area of the solid bead (Diffusion through Reacted Layer)

$$\left[3-3(1-X)^{\frac{2}{3}}-2X\right] = \frac{6D_{e,r}C_{A0}}{ar_0C_{S0}}t \tag{12}$$

c. Chemical reaction of the reacting species with adsorption surface of the zone (Chemical Reaction).

$$\left[1-(1-X)^{\frac{1}{3}}\right] = \frac{k_sC_{A0}}{r_0}t \tag{13}$$

where C_{A0} and C_{As} are concentration of A in bulk solution and on the outer surface of the resin, respectively, r_o represents the bead radius, a is the stoichiometric coefficient, K_{MA} is mass transfer coefficient of species A through the liquid film (m/s), $D_{e,r}$ is effective diffusion coefficient in solid phase (m^2/s) and k_s is the reaction constant based on the surface (m/s).

Functions and transport characteristics of all kinetic models were given in Table 2.

3. Results and discussion

3.1 Characterization of Adsorbsia GTO

Since Adsorbsia GTO has superior arsenic adsorption ability than other adsorbents used, its morphological

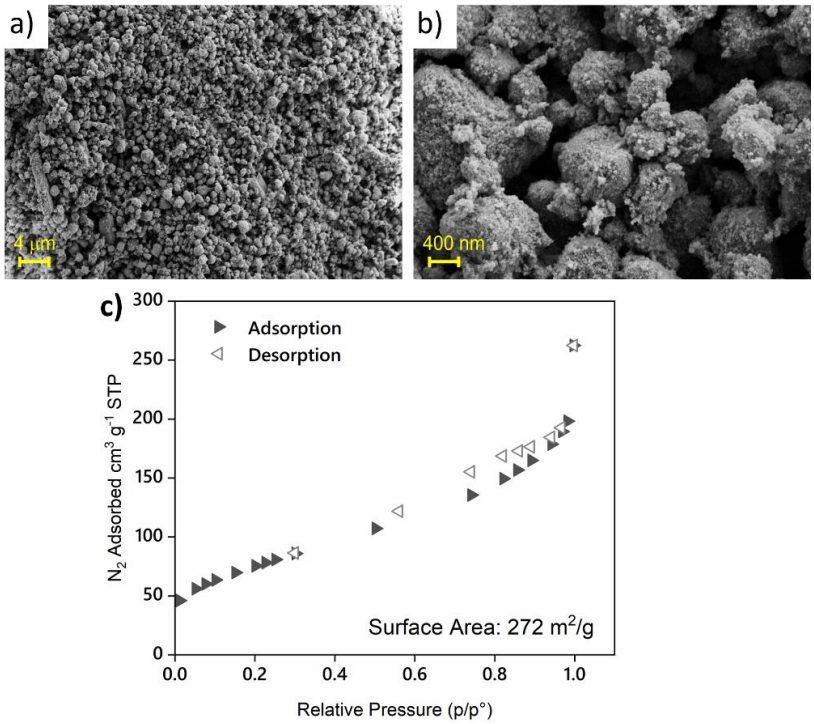

Fig. 5 The properties of Adsorbsia GTO a) SEM image with magnification of 5000x b) SEM image with magnification of 50000x c) Adsorption-Desorption Characteristics

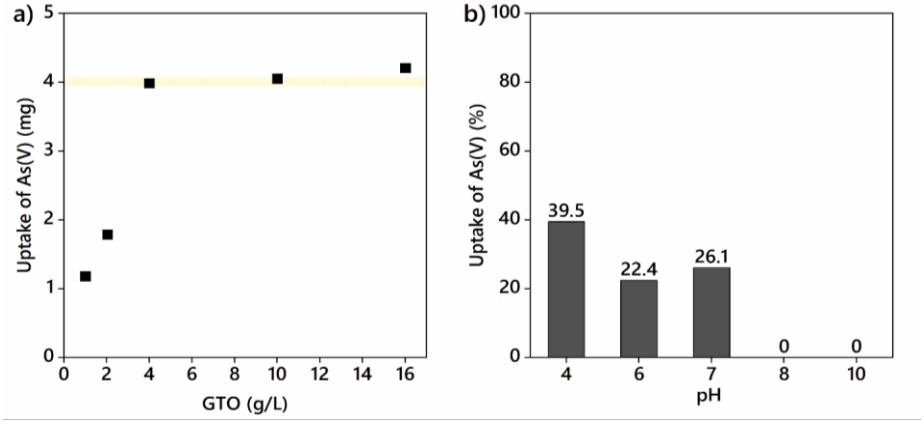

Fig. 6 a) Effect of Adsorbsia GTO amount on the adsorption of As(V) (Particle size: 0.5~0.71 mm, m_{GTO}: 0.05, 0.1, 0.2, 0.5, 0.8 g, pH: 4, T: 25°C, $[As(V)]_0$: 100 ppm, $V_{solution}$: 50 ml) b) Effect of pH on the adsorption of As(V) by Adsorbsia GTO (Particle size: 0.5~0.71 mm, m_{GTO}: 0.1 g, $V_{solution}$:50 ml, T: 25°C, $[As(V)]_0$: 100 ppm)

structure and specific surface area were investigated. SEM analysis was performed to determine the morphological structure of Adsorbsia GTO particles at magnifications of 5000x and 50000x. Figs. 5 (a)-(b) exhibited that Adsorbsia GTO had the agglomerated bead-like shape particles having average diameter of 679 ± 235 nm. Furthermore, the Adsorbsia GTO had small size results in high N_2 adsorption, and the surface area of 272 m^2/g was consistent with the product information (Fig. 5(c)).

3.2 Thermodynamic equilibrium

The preliminary studies were performed to obtain an optimum amount of Adsorbsia GTO. It was found to be 4 g/l for a solution having 100 ppm initial As(V) concentration at pH value of 4 and 25°C as seen in Fig. 6(a).

Because the adsorbent's surface is negatively or positively charged, depending on the solution's pH, this has a big impact on how much arsenic is absorbed during the adsorption process. The effect of pH on sorption behavior was investigated for Adsorbsia GTO and represented in Fig. 6(b). The maximum sorption of As(V) occurred at pH 4 by Adsorbsia GTO whereas there is no sorption observed at pH value of 8 and 10. It is expected that arsenic uptake decreases as the pH increases, since the dominant species become more charged, and one ion occupies more free sites on adsorbent. Therefore, zero uptake cannot be explained with the type of species, but with the behavior of adsorbent. The isoelectric point (IEP), also called as the point of zero charge, for the adsorbents is near neutral, in the pH

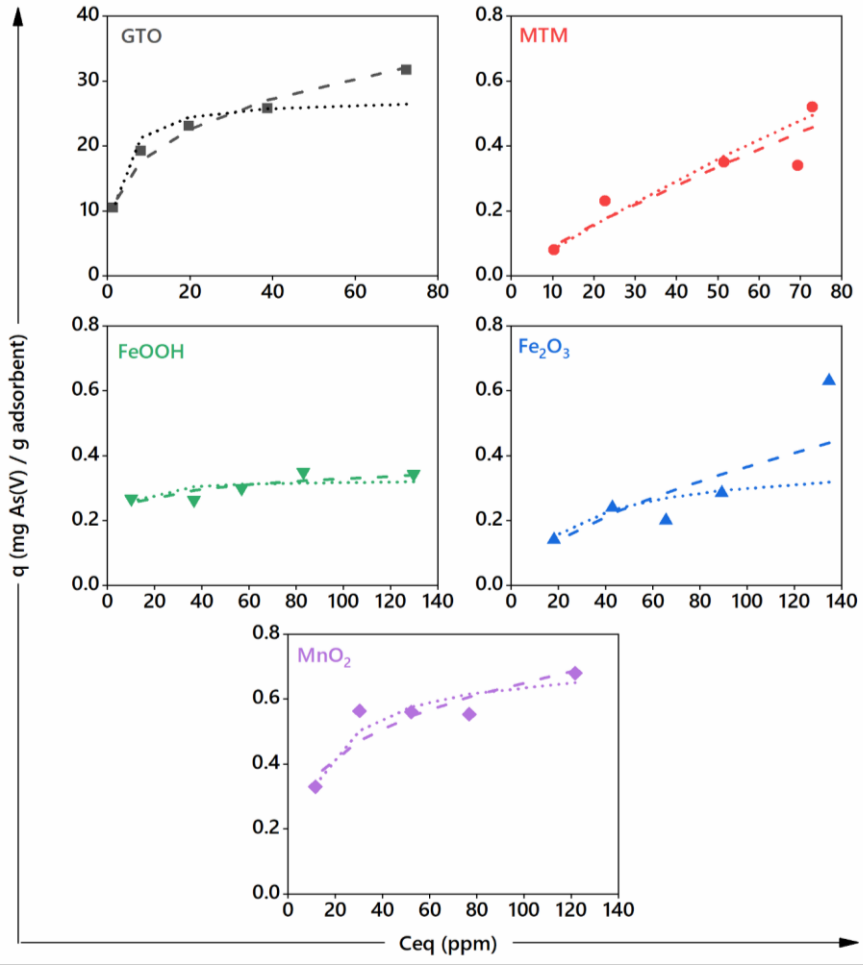

Fig. 7 The equilibrium behavior of adsorbents (pH: 4, T: 25°C, $[As(V)]_0$: 25, 50, 75, 100, 150 ppm). The symbols are shown as ■ GTO ●MTM ▼ FeOOH ▲ Fe_2O_3 ◆ MnO_2 ····· Langmuir Isotherm – – Freundlich Isotherm

range 7–8 (Streat *et al.* 2008). Hence, the surface will attract anions at pH 4 due to the surface being positively charged which is a condition valid for natural oxides. To illustrate, deprotonation at the surface may occur with ligand exchange for protonated anions like arsenate, leading to bidentate inner-sphere bonding.

The degree of positive surface charge reduces with increasing pH, which lessens the forces that attract anionic species. Proton dissociation from the acid surface leads to neutral adsorption. In order to equalize with the solution, adsorbed species take up a proton from it. Notwithstanding the reciprocal repulsion between the negative surface and anionic species, considerable arsenic adsorption occurs at pH > IEP. Therefore, for any adsorption to take place, the energy that the surface gains from creating new bonds with the anion needs to be larger than the repulsive forces. Furthermore, the negative charge of arsenic species increases as arsenate speciates from $H_2AsO_4^-$ to $HAsO_4^{2-}$. If the undissociated acid contributes a proton to the surface hydroxyl group to generate water that can be displaced by the anion, removal at higher pH levels via specific adsorption is feasible (Streat *et al.* 2008).

Experimental data obtained from batch studies were fitted to the Langmuir and Freundlich models in linearized form (Eq. (5) and (7)) to provide the equilibrium isotherms for the commercial and natural adsorbents as seen in Fig. 7.

The models associate the adsorption capacity of As(V) at equilibrium (q_e) with the equilibrium concentration (C_e). Whereas the Freundlich isotherm is appropriate for multilayer adsorption on heterogeneous sites, the Langmuir isotherm is appropriate for monolayer adsorption on homogeneous sites (Kalam *et al.* 2021). Table 3 summarized the results of isotherm parameters and correlation coefficient values (R^2). Surface loading, the quantity of accessible sites and pH affect binding of different arsenic complex to surfaces. The Langmuir model can only provide a limited fit of the data because it does not account for changes in surface charge, speciation, or degree of crystallinity (Gupta and Ghosh 2009).

In this study, both Langmuir and Freundlich isotherms were applied to the adsorption data of different adsorbents. The Freundlich model has a slightly better fit to the equilibrium data of Adsorbsia GTO, while the equilibrium data of MTM® fitted to the Langmuir model. For natural oxides, the equilibrium data of MnO_2 and Fe_2O_3 fitted to the Langmuir model with a correlation coefficient of 0.94, whereas the Freundlich model fitted better the equilibrium data of FeOOH. These linear fits revealed that Adsorbsia GTO and FeOOH have energetically heterogeneous sites for As(V) adsorption. Wang *et al.* (2022) also showed that the

Table 3 Isotherm parameters and R^2 values for adsorption of As(V) for different adsorbents

Adsorbent	$m_{adsorbent}$ (g)	Langmuir Isotherm			Freundlich Isotherm		
		q_{max}	k	R^2	k	n	R^2
GTO	0.1	27.25	0.438	0.97	9.988	3.668	0.98
MTM	0.5	2.77	0.003	0.96	0.014	1.227	0.91
Fe_2O_3	1.0	0.46	0.024	0.77	0.020	1.573	0.76
FeOOH	1.5	0.33	0.385	0.46	0.194	8.703	0.70
MnO_2	1.5	0.72	0.076	0.94	0.187	3.679	0.83

Table 4 Characteristics and correlation coefficients of kinetic models

Adsorbent	Fitting Parameter	Rate Determining Step				
		ISV		UCM		
		Particle Diffusion	Liquid Film Diffusion	Fluid Film Diffusion	Reacted Layer	Chemical Reaction
GTO	Slope	0.00161	0.00333	0.00221	0.00062	0.00096
	R^2	0.95783	0.98913	0.97290	0.95517	0.98619
Fe_2O_3	Slope	0.00296	0.00461	0.00231	0.00111	0.0012
	R^2	0.9404	0.88479	0.75057	0.93944	0.84539
FeOOH	Slope	0.00321	0.00504	0.00257	0.00121	0.00132
	R^2	0.89937	0.90935	0.87885	0.90095	0.90429
MnO_2	Slope	0.00182	0.00363	0.00234	0.00070	0.00104
	R^2	0.97467	0.96666	0.92564	0.97315	0.95505

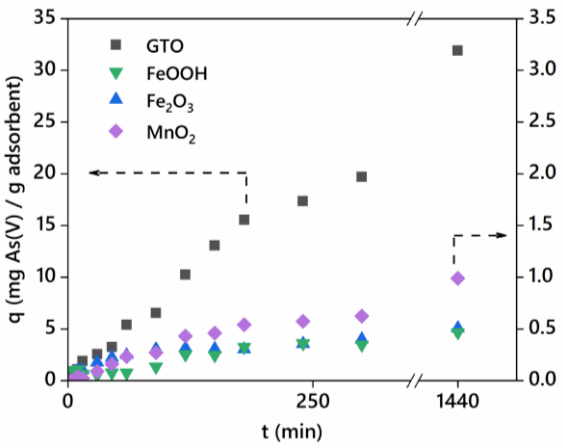

Fig. 8 Kinetic behavior of the different adsorbents for As(V) adsorption ([As(V)]$_0$: 100 ppm, T: 25 ºC, pH: 4)

best fit isotherm among Langmuir, Freundlich and Temkin Isotherms is Freundlich Isotherm which supports this study.

According to applied models, the adsorption capacities of MTM®, Fe_2O_3, FeOOH and MnO_2 were calculated as 2.77, 0.46, 0.33, and 0.72 mg As(V)/g adsorbent, respectively. Whereas the adsorption capacity of Adsorbsia GTO as a commercial adsorbent has the highest value as 27.25 mg As(V)/g adsorbent and it is comparable with 28.5 mg/g of arsenic adsorption capacity found by Hristovski *et al.* (2008) while the manufacturer data represents 12-15 mg As(V)/g adsorbent as an adsorption capacity of Adsorbsia GTO. In addition, MnO_2 was found to have the highest adsorption capacity among natural adsorbents.

3.3 Sorption kinetics with particle

A series of batch experiments have been performed to investigate the kinetic mechanisms of As(V) sorption onto Adsorbsia GTO and natural mineral oxides. The *q* values were calculated from initial and final concentration differences between initial and any time *t* as seen in Fig. 8. The *q* values of Adsorbsia GTO were exhibited in the primary Y-axis whereas *q* values of other adsorbents were shown in the second Y-axis due to the high adsorption capacity differences.

Kinetic models named “Infinite Solution Volume (ISV)” and “Unreacted Core Model (UCM)” were subjected to the experimental data of different adsorbents. The kinetic data was plotted in Fig. 9 and the fitting parameters were represented in Table 4. It indicated that the rate determining step was the liquid film diffusion control for both Adsorbsia GTO and FeOOH whereas it was the particle diffusion control for the sorption by Fe_2O_3 and MnO_2 according to the Infinite Solution Volume Diffusion Model. On the other hand, the rate determining step was the chemical reaction control for both Adsorbsia GTO and FeOOH whereas it was the reacted layer control for the sorption by Fe_2O_3 and MnO_2 with respect to the Unreacted Shrinking Core Model. Considering Adsorbsia GTO and FeOOH both fitting the liquid film diffusion (ISV) and the reacted layer (UCM), the concentration difference on the outside of adsorbent is controlling the adsorption process. While the controlling step for Fe_2O_3 and MnO_2 is the concentration inside the adsorbent and outer layer of the adsorbent.

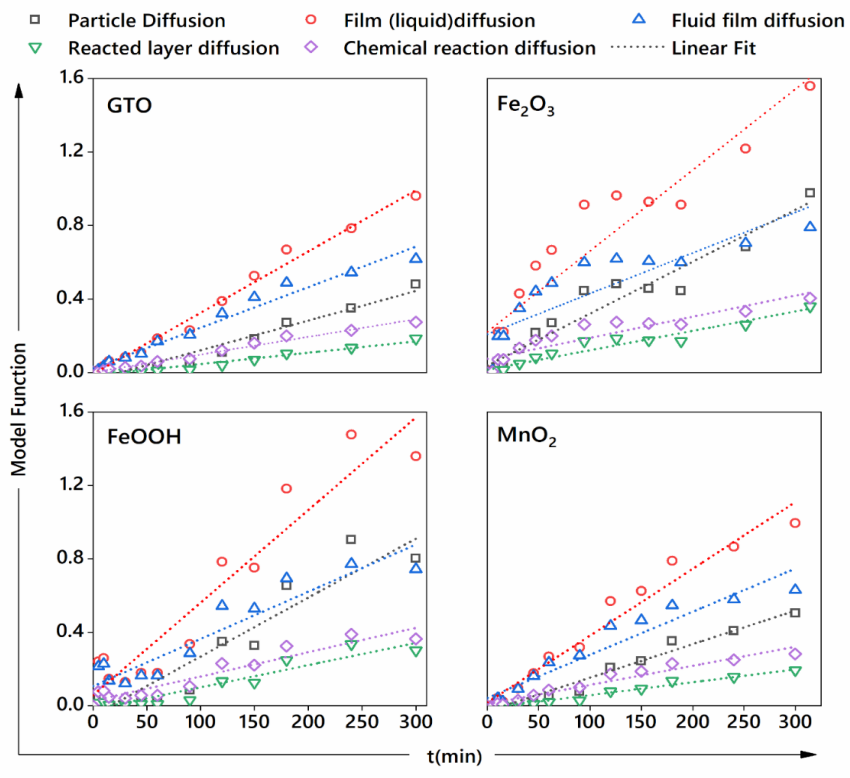

Fig. 9 Kinetic model fitting for As(V) adsorption on different adsorbents

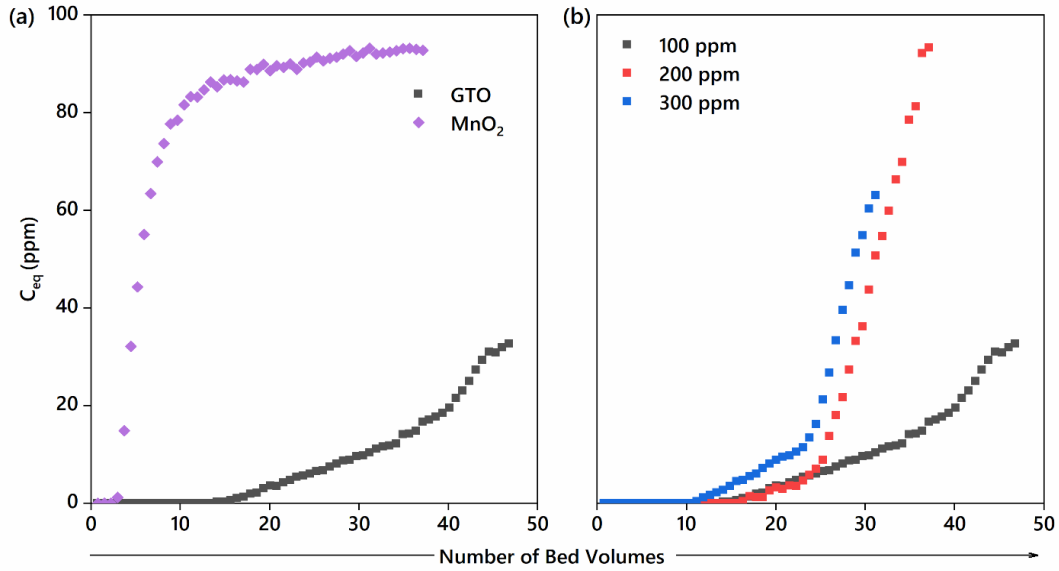

Fig. 10 Breakthrough curves for (a) Adsorbsia GTO and MnO_2 (pH: 4, Flowrate: 8.6 BV/h, $[As(V)]_0$:100 ppm, Vcolumn:14 ml) (b) Adsorbsia GTO at different initial concentrations (V_{GTO}: 14 ml, pH: 4, Flowrate: 8.6 BV/h, $[As(V)]_0$: 100, 200, 300 ppm)

3.4 Sorption kinetics in column

Based on batch sorption results, continuous experiments were carried out to obtain the breakthrough characteristics of commercial and natural adsorbents, Adsorbsia GTO and MnO_2 as seen in Fig. 10. The breakthrough exchange capacities were determined as the total amount of effluent with no arsenic.

For the removal of As(V), the breakthrough and total exchange capacities of the Adsorbsia GTO and MnO_2 were tabulated in Table 5. The breakthrough and total capacities of Adsorbsia GTO and MnO_2 were obtained as 26.5, 84.4 mg/ml and 4.3, 14.2 mg/ml for 100 ppm initial concentration of As(V), respectively. Adsorbsia GTO exhibited higher breakthrough and total exchange capacities than MnO_2. However, the percentages of column utilization were the same for both promising adsorbents.

Overall, Adsorbsia GTO exhibits superior performance

Table 5 The breakthrough (BEC), total capacities (TEC) and percentages of column utilization (CU%) values of Adsorbsia GTO and MnO_2 in As(V) removal in the column studies (C_0: 100 ppm As(V), pH: 4, Flowrate: 8.6 BV/h)

Adsorbents	*BEC [mg/mL]	**TEC [mg/mL]	CU [%]
GTO	26.5	84.4	31
MnO_2	4.3	14.2	30

than natural oxides. According to isotherm and kinetics results, it fits with multilayer adsorption and the adsorption is controlled by the concentration in the liquid film outside of the adsorbent. Hence, it is better to use Adsorbsia GTO for high arsenic concentrated water bodies. In contrast to that, MnO_2 having less capacity and the rate limiting step being the concentration inside the adsorbent, would not be a good choice for high concentration and high amount of water bodies. However, both Adsorbsia GTO and MnO_2 have column utilization around 30% which shows that both have the same efficiency. In practice, the same amount of arsenic adsorption can be achieved by using more MnO_2 than Adsorbsia GTO or frequent cleaning of the MnO_2 adsorbent column would work as well.

4. Conclusions

The equilibrium and kinetics studies were conducted on both commercially available and natural mineral oxides adsorbents to understand the use of natural mineral oxides as a potential adsorbent in adsorption of arsenic from the water.

• The maximum adsorption capacity of Adsorbsia GTO was found to be 27.25 mg As(V)/g adsorbent from Langmuir Isotherm, the high adsorption capacity occurred at pH 4 because only one species, [$H_2AsO_4^-$] existed in the water and Adsorbsia GTO was best fitted to Freundlich Isotherm.

• The adsorption capacity of MTM® was 2.77 mg As(V)/g adsorbent and it was better fitted to the Langmuir model. The arsenic adsorption capacities of natural minerals, such as Fe_2O_3, FeOOH and MnO_2, were 0.46, 0.33, and 0.72 mg As(V)/g adsorbent, respectively. While the equilibrium data of manganese dioxide and hematite was fitted to the Langmuir model, the Freundlich model better fitted equilibrium data of goethite.

• While the rate determining step was the liquid film diffusion control and chemical reaction control for both Adsorbsia GTO and FeOOH, it was the particle diffusion control and the reacted layer control for the sorption by Fe_2O_3 and MnO_2.

• The study reveals the small adsorption capacity of MnO_2 is inhibited by interparticle arsenic concentration and diffusion of it.

• Column studies were carried out on Adsorbsia GTO, a superior commercial adsorbent, and manganese oxide (MnO_2), a promising natural mineral. The breakthrough and total capacities of Adsorbsia GTO were 26.5 and 84.4 mg/ml whereas these capacities of MnO_2 were obtained as 4.3 and 14.2 mg/ml for 100 ppm initial concentration of As(V).

• Adsorbsia GTO exhibited higher breakthrough and total exchange capacities than MnO_2. However, the percentages of column utilization were almost the same as 30% for both promising adsorbents.

• In a broad perspective, although natural oxides do not have as high capacities as commercial ones, it makes them readily available and cost-effective adsorbents for water with low arsenic levels.

Acknowledgement

This study was supported by Ege University Research Foundation by contract no: 09MÜH052.

References

Abdul, K.S.M., Jayasinghe, S.S., Chandana, E.P.S., Jayasumana, C., De Silva and P.M.C.S. (2015), "Arsenic and human health effects: A review", *Environ. Toxicol. Pharmacol*., **40**(3), 828-846. https://doi.org/10.1016/j.etap.2015.09.016

Aitbelale, R., Timesli, A. and Sahibed-dine, A. (2023), "Functional graphene sheets-TiO2 nanocomposites and their photocatalytic performance for wastewater treatment", *Adv. Nano Res*., **15**(4), 295-304. https://doi.org/10.12989/anr.2023.15.4.295

Alka, S., Shahir, S., Ibrahim, N., Ndejiko, M.J., Vo, D.V.N. and Manan, F.A. (2021), "Arsenic removal technologies and future trends: A mini review", *J. Clean. Prod*., **278**. https://doi.org/10.1016/j.jclepro.2020.123805

Altowayti, W.A.H., Othman, N., Shahir, S., Alshalif, A.F., Al-Gheethi, A.A., AL-Towayti, F.A.H., Saleh, Z.M. and Haris, S.A. (2022), "Removal of arsenic from wastewater by using different technologies and adsorbents: A review", *Int. J. Environ. Sci. Technol*., **19**(9), 9243-9266. https://doi.org/10.1007/s13762-021-03660-0

Carneiro, M.A., Pintor, A.M.A., Boaventura, R.A.R. and Botelho, C.M.S. (2022), "Efficient removal of arsenic from aqueous solution by continuous adsorption onto iron-coated cork granulates", *J. Hazard. Mater*., **432**. https://doi.org/10.1016/j.jhazmat.2022.128657

Chen, Y.W., Yu, X. and Belzile, N. (2019), "Arsenic speciation in surface waters and lake sediments in an abandoned mine site and field observations of arsenic eco-toxicity", *J. Geochem. Explor*., **205**, 106349. https://doi.org/10.1016/j.gexplo.2019.106349

Choong, T.S.Y., Chuah, T.G., Robiah, Y., Gregory Koay, F.L. and Azni, I. (2007), "Arsenic toxicity, health hazards and removal techniques from water: An overview", *Desalination*, **217**(1-3), 139-166. https://doi.org/10.1016/j.desal.2007.01.015

DeMarco, M.J., SenGupta, A.K., Greenleaf, J.E. (2003), "Arsenic removal using a polymeric/inorganic hybrid sorbent", *Water Res*., **37**(1), 164-176. https://doi.org/10.1016/S0043-1354(02)00238-5

Diephuis, W.R., Molloy, A.L., Boltz, L.L., Porter, T.B., Orozco, A.A., Duron, R., Crespo, D., George, L.J., Reiffer, A.D., Escalera, G., Bohloul, A., Avendano, C., Colvin, V.L. and Gonzalez-Pech, N.I. (2022), "The effect of agglomeration on arsenic adsorption using iron oxide nanoparticles", *Nanomaterials*, **12**(9), 1598. https://doi.org/10.3390/nano12091598

Dow Chemical Company, "Adsorbsia™ GTO™ titanium Based Media", Product Information, Form No. 177-02044-0506. https://www.lenntech.com/Data-sheets/Adsorbsia%20GTO.pdf.

Dutta, P.K., Ray, A.K., Sharma, V.K. and Millero, F.J. (2004), "Adsorption of arsenate and arsenite on titanium dioxide

suspensions", *J. Colloid Interf. Sci*., **278**(2), 270-275. https://doi.org/10.1016/j.jcis.2004.06.015

Eddy, N.O., Garg, R., Garg, R., Eze, S.I., Ogoko, E.C., Kelle, H.I., Ukpe, R.A. and Ogbodo, R., Chijoke, F. (2023), "Sol-gel synthesis, computational chemistry, and applications of Cao nanoparticles for the remediation of methyl orange contaminated water", *Adv. Nano Res*., **15**(1), 35-48. https://doi.org/10.12989/anr.2023.15.1.035

Fu, L., Li, J., Yang, J., Liu, Y., He, C. and Chen, Y. (2023), "Purification process and reduction of heavy metals from industrial wastewater via synthesized nanoparticle for water supply in swimming/water sport", *Adv. Nano Res*., **15**(5), 441-449. https://doi.org/10.12989/anr.2023.15.5.441

Giménez, J., Martínez, M., de Pablo, J., Rovira, M. and Duro, L. (2007), "Arsenic sorption onto natural hematite, magnetite, and goethite", *J. Hazard. Mater*., **141**(3), 575-580. https://doi.org/10.1016/j.jhazmat.2006.07.020

Gupta, K. and Ghosh, U.C. (2009), "Arsenic removal using hydrous nanostructure iron(III)-titanium(IV) binary mixed oxide from aqueous solution", *J. Hazard. Mater*., **161**(2-3), 884-892. https://doi.org/10.1016/j.jhazmat.2008.04.034

Haron, M.J., Shiah, L.L. and Yunus W.M.Z. (2006), "Sorption of arsenic (V) by titanium oxide loaded poly(hydroxamic acid) resin", *Malaysian J. Anal. Sci*., **10**(2), 261-268.

Hristovski, K., Westerhoff, P., Möller, T., Sylvester, P., Condit, W. and Mash, H. (2008), "Simultaneous removal of perchlorate and arsenate by ion-exchange media modified with nanostructured iron (hydr)oxide", *J. Hazard. Mater*., **152**(1), 397-406. https://doi.org/10.1016/j.jhazmat.2007.07.016

Iesan, C.M., Capat, C., Ruta, F. and Udrea, I. (2008), "Evaluation of a novel hybrid inorganic/organic polymer type material in the arsenic removal process from drinking water", *Water Res*., **42**(16), 4327-4333. https://doi.org/10.1016/j.watres.2008.06.011

Jeon, C.S., Baek, K., Park, J.K., Oh, Y.K. and Lee, S.D. (2009), "Adsorption characteristics of As(V) on iron-coated zeolite", *J. Hazard. Mater*., **163**(2–3), 804-808. https://doi.org/10.1016/j.jhazmat.2008.07.052

Kabay, N., Gizli, N., Demircioğlu, M., Yuksel, M., Jyo, A., Yamabe, K. and Shuto, T. (2003), "Cr(III) removal by macroreticular chelating ion exchange resins", *Chem. Eng. Commun*., **190**(5-8), 813-822. https://doi.org/10.1080/00986440302114

Kalam, S., Abu-Khamsin, S.A., Kamal, M.S. and Patil, S. (2021), "Surfactant adsorption isotherms: A review", *ACS Omega*, **6**(48), 32342-32348. https://doi.org/10.1021/acsomega.1c04661

Katsoyiannis, I.A. and Zouboulis, A.I. (2002), "Removal of arsenic from contaminated water sources by sorption onto iron-oxide-coated polymeric materials", *Water Res*., **36**(20), 5141-5155. https://doi.org/10.1016/S0043-1354(02)00236-1

Kundu, S. and Gupta, A.K. (2007), "Adsorption characteristics of As(III) from aqueous solution on iron oxide coated cement (IOCC)", *J. Hazard. Mater*., **142**(1-2), 97-104. https://doi.org/10.1016/j.jhazmat.2006.07.059

Mamindy-Pajany, Y., Hurel, C., Marmier, N. and Roméo, M. (2011), "Arsenic (V) adsorption from aqueous solution onto goethite, hematite, magnetite and zero-valent iron: effects of pH, concentration and reversibility", *Desalination*, **281**(1), 93-99. https://doi.org/10.1016/j.desal.2011.07.046

Mandal, B.K. and Suzuki, K.T. (2002), "Arsenic round the world: a review", *Talanta*, **58**, 201-235. https://doi.org/10.1016/S0065-2113(08)70013-0

Mayo, J.T., Yavuz, C., Yean, S., Cong, L., Shipley, H., Yu, W., Falkner, J., Kan, A., Tomson, M. and Colvin, V.L. (2007), "The effect of nanocrystalline magnetite size on arsenic removal", *Sci. Technol. Adv. Mater.*, **8**(1-2), 71-75. https://doi.org/10.1016/j.stam.2006.10.005

McGeogh, M., Annath, H. and Mangwandi, C. (2024), "Turning teawaste particles into magnetic bio-sorbents particles for arsenic removal from wastewater: Isotherm and kinetic studies", *Particuology*, **87**, 179-193. https://doi.org/10.1016/j.partic.2023.08.003

Mehryar, M. and Marandi, G. (2024), "A highly effective route for removal of Hg2+ from the waste water using 3-nitrobenzelidenemalononitrile as a modifier of Fe3O4@SiO2 nanoparticles", *Adv. Nano Res*., **16**(1), 1-9. https://doi.org/10.12989/anr.2024.16.1.001

Mohan, D. and Pittman, C.U. (2007), "Arsenic removal from water/wastewater using adsorbents-a critical review", *J. Hazard. Mater*., **142**(1-2), 1-53. https://doi.org/10.1016/j.jhazmat.2007.01.006

Möller, T. and Sylvester, P. (2008), "Effect of silica and pH on arsenic uptake by resin/iron oxide hybrid media", *Water Res*., **42**(6-7), 1760-1766. https://doi.org/10.1016/j.watres.2007.10.044

Nabi, D., Aslam, I. and Qazı, I.A. (2009), "Evaluation of the adsorption potential of titanium dioxide nanoparticles for arsenic removal", *J. Environ. Sci*., **21**(3), 402-408. https://doi.org/10.1016/S1001-0742(08)62283-4

Pan, B., Pan, B., Zhang, W., Lv, L., Zhang, Q. and Zheng, S. (2009), "Development of polymeric and polymer-based hybrid adsorbents for pollutants removal from waters", *Chem. Eng. J*., **151**(1-3), 19-29. https://doi.org/10.1016/j.cej.2009.02.036

Pena, M.E., Korfiatis, G.P., Patel, M., Lippincott, L. and Meng, X. (2005), "Adsorption of As(V) and As(III) by nanocrystalline titanium dioxide", *Water Res*., **39**(11), 2327-2337. https://doi.org/10.1016/j.watres.2005.04.006

Ruthven, D.M. (1984), *Principle of Adsorption and Adsorption Process*, In *Principles of Adsorption and Adsorption Processes*, **19**, 433, John Wiley and Sons.

Smedley, P.L. and Kinniburgh, D.G. (2002), "A review of the source, behaviour and distribution of arsenic in natural water", *Appl. Geochem*., **17**, 517-568. https://doi.org/10.1016/S0883-2927(02)00018-5

Streat, M., Hellgardt, K. and Newton, N.L.R. (2008), "Hydrous ferric oxide as an adsorbent in water treatment. Part 2. adsorption studies", *Proc. Safe. Environ. Protect*., **86**(1B), 11-20. https://doi.org/10.1016/j.psep.2007.10.008

Ungureanu, G., Santos, S., Boaventura, R. and Botelho, C. (2015), "Arsenic and antimony in water and wastewater: overview of removal techniques with special reference to latest advances in adsorption", *J. Environ. Manage*., **151**, 326-342. https://doi.org/10.1016/j.jenvman.2014.12.051

van Halem, D., Bakker, S.A., Amy, G.L., van Dijk, J.C. (2009), "Arsenic in drinking water: A worldwide water quality concern for water supply companies", *Drinking Water Eng. Sci*., **2**(1), 29-34. https://doi.org/10.5194/dwes-2-29-2009

Wang, Y., Zhang, L., Guo, C., Gao, Y., Pan, S., Liu, Y., Li, X. and Wang, Y. (2022), "Arsenic removal performance and mechanism from water on iron hydroxide nanopetalines", *Sci. Rep*., **12**(1), 1-15. https://doi.org/10.1038/s41598-022-21707-1

WHO. (2022), *Guidelines for Drinking-Water Quality*, In *World Health Organization*.

Xu, Z. and Meng, X. (2009), "Size effects of nanocrystalline TiO2 on As(V) and As(III) adsorption and As(III) photooxidation", *J. Hazard. Mater*., **168**(2-3), 747-752. https://doi.org/10.1016/j.jhazmat.2009.02.084

Zhang, Y., Yang, M. and Huang, X. (2003), "Arsenic(V) removal with a Ce(IV)-doped iron oxide adsorbent", *Chemosphere*, **51**(9), 945-952. https://doi.org/10.1016/S0045-6535(02)00850-0

CC